

A DATA-BASED IMAGE REPRESENTATION FOR CONTINUOUS-TIME LTI SYSTEMS

AMINE OTHMANE[†], PHILIPP SCHMITZ[†], KARL WORTHMANN,
AND KATHRIN FLASSKAMP

ABSTRACT. We derive a numerically stable method to obtain an image representation of an unknown linear system only from data, leveraging a continuous-time version of Willems et al.'s fundamental lemma. We propose a data-based representation that, unlike previous approaches, avoids solving differential-algebraic equations and uses derivatives approximated by algebraic differentiators. Our image-based formulation significantly reduces the complexity of the data-driven representation by eliminating redundant degrees of freedom and thus reducing the number of unknown quantities to be identified. Simulation results confirm the effectiveness of the proposed approach, even in the presence of severe measurement disturbances.

1. INTRODUCTION

The design of controllers and feedback laws directly from data, commonly referred to as direct data-driven control (see, e.g., [4]), has attracted considerable research interest in recent years. A key result in this field is the fundamental lemma by Willems et al. [19]. This lemma states that all finite-length trajectories of a controllable discrete-time linear time-invariant (LTI) system can be parameterized using input–output data arranged in a Hankel matrix, provided suitable persistency of excitation conditions are met. This result has enabled numerous applications in direct data-driven control, for example in [3] and [2]; see [10] and [5] for comprehensive overviews.

Several continuous-time extensions have been developed. The approach in [8] uses Hankel-like structures from sampled trajectories, while [16] provides an approximate fundamental lemma based on orthogonal polynomials. Input–output versions were proposed in [9] by stacking time-shifted signals, and in [17] by introducing a Gramian-based framework involving jets of trajectories. Only the latter two avoid state measurements, but pose other challenges from an applicational point of view. While in discrete time, trajectories are obtained directly as a matrix–vector product with a Hankel data matrix, the continuous-time approaches in [9] and [17] require solving a differential-algebraic equation. Moreover, these methods depend on higher-order derivatives of an informative trajectory, which are typically unknown and must be estimated from noisy measurements. Computing derivatives from noisy data is challenging, as it constitutes an ill-posed problem.

In this paper, we address the two main challenges discussed above, namely the need to solve differential-algebraic equations and the estimation of higher-order

[†]Both authors contributed equally to this work. A. Othmane is grateful for the support from the German Federal Ministry of Research, Technology and Space (No. 05M22TSA). P. Schmitz is grateful for the support from the Carl Zeiss Foundation (VerneDCt – No. 2011640173).

derivatives from noisy measurements. Based on the result in [17], we first derive an image-based, data-driven formulation for controllable continuous-time LTI systems, cf. [18]. This representation circumvents the need to solve differential-algebraic equations and reduces the complexity of the data-based trajectory parameterization by removing redundant degrees of freedom, thereby fewer unknowns must be identified. Second, we incorporate algebraic differentiators introduced in [11] to reliably estimate the required derivatives from measured data. These differentiators provide an efficient and robust approach, as evidenced by the diverse applications summarized in [14], which also contains tuning guidelines. Moreover, an open-source software toolbox accompanied by a practical introduction can be found in [15]. We show that the estimated signals preserve the persistency of excitation property required by the fundamental lemma. We restrict attention to single-output systems and develop the method in this setting. Simulation results demonstrate the effectiveness of the approach, even in the presence of substantial measurement disturbances.

The paper is organized as follows. Section 2 formalizes the problem setting and recalls the concepts of persistency of excitation and the continuous-time fundamental lemma. In Section 3, we develop a method to construct an image representation from noisy data. Section 4 illustrates the theoretical findings using numerical simulations before conclusions are drawn in Section 5. Supplementary material on algebraic differentiators, including the definition of suitable filter kernels, is provided in Appendix A.

Notation: Given an interval $\mathcal{I} \subset \mathbb{R}$ and $d \in \mathbb{N} \setminus \{0\}$, the space of equivalence classes of square integrable functions from \mathcal{I} to \mathbb{R}^d is denoted by $L^2(\mathcal{I}, \mathbb{R}^d)$. The associated Sobolev space of order $k \in \mathbb{N}$ is denoted by $H^k(\mathcal{I}, \mathbb{R}^d)$. The convolution of two integrable functions is defined as $(f * g)(t) := \int_{\mathbb{R}} f(s)g(t - s) ds$, where functions defined on an interval $\mathcal{I} \subset \mathbb{R}$ are extended by zero outside of \mathcal{I} . For a sufficiently smooth function $x : \mathcal{I} \rightarrow \mathbb{R}$, we denote by $x^{(i)}$ its i -th derivative, with the convention $x^{(0)} = x$; we also write $\dot{x} = x^{(1)}$. For matrices or vectors A_1, \dots, A_n of compatible size we write $\text{col}(A_1, \dots, A_n) := [A_1^\top \ \dots \ A_n^\top]^\top$. This notation extends to matrix-valued (resp. vector-valued) functions. The notation $\text{Unif}([-a, a])$ with $a > 0$, refers to the uniform distribution on the interval $[-a, a]$.

2. SETTING AND PROBLEM DESCRIPTION

In this section we introduce the problem setting and recall the continuous-time fundamental lemma.

2.1. Linear time-invariant systems. We focus on continuous-time LTI systems of the form

$$\begin{aligned} \dot{x}(t) &= Ax(t) + Bu(t) \\ y(t) &= Cx(t) + Du(t) \end{aligned} \tag{1}$$

on an open and finite time interval \mathcal{I} with system matrices $A \in \mathbb{R}^{n \times n}$, $B \in \mathbb{R}^{n \times m}$, $C \in \mathbb{R}^{p \times n}$ and $D \in \mathbb{R}^{p \times m}$. At time $t \in \mathcal{I}$, the state, the input, and the output of the system are given by $x(t) \in \mathbb{R}^n$, $u(t) \in \mathbb{R}^m$ and $y(t) \in \mathbb{R}^p$, respectively. As the set of valid input–output trajectories corresponding to system (1), we consider the *behavior*

$$\mathcal{B} := \left\{ \text{col}(u, y) \in L^2(\mathcal{I}, \mathbb{R}^{m+p}) \left| \begin{array}{l} \exists x \in H^1(\mathcal{I}, \mathbb{R}^n) \text{ s.t.} \\ (1) \text{ holds a.e. in } \mathcal{I} \end{array} \right. \right\}.$$

The behavior \mathcal{B} is a closed linear subspace in $L^2(\mathcal{I}, \mathbb{R}^{m+p})$, cf. [17, Lem. 2 and Lem. 3].

In the following we suppose that the state-space representation in (1) is minimal, that is, system (1) is both controllable and observable. For algebraic conditions equivalent to controllability and observability, see e.g., [18, Section 5]. Controllability is equivalent to the existence of an *image representation* of the behavior, see [18, Theorem 6.6.1] and [17, Lemma 6] for the setting of closed L^2 -subspaces. Accordingly, there is a polynomial matrix $M \in \mathbb{R}^{(m+p) \times m}[s]$ with $M(s) = \sum_{k=0}^{n+1} M_k s^k$ such that

$$\mathcal{B} = \left\{ w \in L^2(\mathcal{I}, \mathbb{R}^{m+p}) \left| \begin{array}{l} \exists \ell \in L^2(\mathcal{I}, \mathbb{R}^m) \text{ s.t.} \\ w = M\left(\frac{d}{dt}\right)\ell \text{ a.e. in } \mathcal{I} \end{array} \right. \right\}. \quad (2)$$

The variable ℓ in (2), called the *latent variable*, is a differentially flat output of system (1). The equation $M\left(\frac{d}{dt}\right)\ell = w$ should be interpreted in the weak sense, i.e.

$$\int_{\mathcal{I}} w^{\top}(s) \phi(s) ds = \sum_{k=0}^n (-1)^k \int_{\mathcal{I}} \ell(s)^{\top} M_k^{\top} \phi^{(k)}(s) ds \quad (3)$$

for every infinitely differentiable function $\phi : \mathcal{I} \rightarrow \mathbb{R}^m$ with compact support. For any k -times continuously differentiable $\ell : \mathcal{I} \rightarrow \mathbb{R}^m$, the pointwise equation $M\left(\frac{d}{dt}\right)\ell = w$ is equivalent to (3), which follows by integration by parts.

An important quantity associated with \mathcal{B} is the *lag* $\mathfrak{l}(\mathcal{B})$ (see [18]), which coincides with the observability index of (1), i.e. the smallest integer $k \geq 1$ such that $\text{rank} [C^{\top} \ (CA)^{\top} \ \dots \ (CA^{k-1})^{\top}] = n$.

2.2. A data-driven representation. In the following, we recall the concept of *persistency of excitation* and the fundamental lemma for continuous-time LTI systems from [17].

Definition 1. A function $u : \mathcal{I} \rightarrow \mathbb{R}^m$ is called persistently exciting of order k , $k \in \mathbb{N} \setminus \{0\}$, if $u \in H^{k-1}(\mathcal{I}, \mathbb{R}^m)$ and the set of the $k \cdot m$ scalar components of $\text{col}(u, \dots, u^{(k-1)})$ is linearly independent in the space $L^2(\mathcal{I}, \mathbb{R})$.

Lemma 2 (Fundamental lemma). Suppose system (1) is controllable, and let $(\bar{u}, \bar{y}) \in \mathcal{B}$ be such that \bar{u} is persistently exciting of order $L + n + 1$ for some $L \geq \mathfrak{l}(\mathcal{B})$. Define the Gramian matrix

$$\Gamma := \int_{\mathcal{I}} \bar{W}(s) \bar{W}^{\top}(s) ds \in \mathbb{R}^{L(m+p) \times L(m+p)}$$

for $\bar{W} = \text{col}(\bar{u}, \dots, \bar{u}^{(L-1)}, \bar{y}, \dots, \bar{y}^{(L-1)})$. Then, $\text{col}(u, y) \in H^{L-1}(\mathcal{I}, \mathbb{R}^{m+p})$ is an element of \mathcal{B} if and only if there exists $\mathfrak{g} \in L^2(\mathcal{I}, \mathbb{R}^{L(m+p)})$ satisfying

$$\text{col}(u, \dots, u^{(L-1)}, y, \dots, y^{(L-1)}) = \Gamma \mathfrak{g}. \quad (4)$$

Moreover, $\text{rank } \Gamma = Lm + n$.

Remark 3. In (4), Γ may be replaced by any matrix $\tilde{\Gamma}$ with $\text{im } \tilde{\Gamma} = \text{im } \Gamma$, with \mathfrak{g} taken in the corresponding L^2 -space, cf. [17, Rem. 23].

The fundamental lemma allows for a complete description of the system's behavior by means of the data matrix Γ . This can be used, e.g., for data-based system simulation or in developing direct data-based control algorithms.

Unlike the discrete-time fundamental lemma by [19], where finite-horizon trajectories are obtained directly via a matrix–vector product, the continuous-time case in (4) requires solving a differential-algebraic equation. Using the decomposition

$$\Gamma = \text{col}(\Gamma_{\bar{u}^{(0)}}, \dots, \Gamma_{\bar{u}^{(L-1)}}, \Gamma_{\bar{y}^{(0)}}, \dots, \Gamma_{\bar{y}^{(L-1)}}) \quad (5)$$

with $\Gamma_{\bar{u}^{(k)}} \in \mathbb{R}^{m \times L(m+p)}$, $\Gamma_{\bar{y}^{(k)}} \in \mathbb{R}^{p \times L(m+p)}$ for $k \in \{0, \dots, L-1\}$, we obtain the equivalence of (4) to $\text{col}(u, y) = \text{col}(\Gamma_{\bar{u}^{(0)}}, \Gamma_{\bar{y}^{(0)}})\mathbf{g}$ together with

$$\frac{d}{dt}(E_0\mathbf{g}) = A_0\mathbf{g}, \quad (6)$$

where

$$E_0 = \begin{bmatrix} \Gamma_{\bar{u}^{(0)}} \\ \vdots \\ \Gamma_{\bar{u}^{(L-2)}} \\ \Gamma_{\bar{y}^{(0)}} \\ \vdots \\ \Gamma_{\bar{u}^{(L-2)}} \end{bmatrix}, \quad A_0 = \begin{bmatrix} \Gamma_{\bar{u}^{(1)}} \\ \vdots \\ \Gamma_{\bar{u}^{(L-1)}} \\ \Gamma_{\bar{y}^{(1)}} \\ \vdots \\ \Gamma_{\bar{u}^{(L-1)}} \end{bmatrix}. \quad (7)$$

In the following, we derive an image representation as in (2) from the data-based representation (4). Our representation eliminates the need to solve the differential-algebraic equation (6) and, at the same time, removes redundancies in the data-based description. While $\ell \in L^2(\mathcal{I}, \mathbb{R}^m)$ in (2), \mathbf{g} is required to belong to $L^2(\mathcal{I}, \mathbb{R}^{L(m+p)})$ in (4), introducing redundant degrees of freedom.

3. IMAGE REPRESENTATION FROM NOISY DATA

In the following, we present a procedure for deriving an image representation (2) from the data-driven model (4), starting from nominal data and then extending the approach to estimated derivatives from noisy measurements.

3.1. Unimodular embedding. A key step, based on nominal data, is to embed the pencil $sE_0 - A_0$ (associated with the differential-algebraic equation (6)) into a unimodular polynomial matrix. A polynomial matrix G is called *unimodular* if it is square and invertible over the ring of polynomial matrices.

The required embedding therefore consists of finding a polynomial matrix K such that G with

$$G(s) = [sE_0^\top - A_0^\top \quad K^\top(s)]^\top \quad (8)$$

is unimodular.

Proposition 4 ([1, Cor. 1]). *A matrix pencil $sE_0 - A_0$ has a unimodular embedding (8) if and only if it has full row rank for all $s \in \mathbb{C}$. In this case, there exists a unimodular embedding with constant K .*

In the following, we restrict our attention to the single-output case ($p = 1$), which simplifies the analysis. In this case, the lag $\mathbf{l}(\mathcal{B})$ and the observability index both equal the system order n .

Corollary 5. *Assume $p = 1$ and let the assumptions of Lemma 2 hold with $L = \mathbb{I}(\mathcal{B}) = n$. Then the matrix pencil $sE_0 - A_0$ associated with (6) has a unimodular embedding (8) with constant K .*

Proof. Since $L = n$ and $p = 1$, the data matrix Γ has full row rank by Lemma 2. Observe that $sE_0 - A_0 = (sJ_1 - J_2)\Gamma$, where J_1 and J_2 are defined as

$$J_1 = \begin{bmatrix} I_{(L-1)m} & 0 & 0 \\ 0 & 0 & I_{(L-1)p} \end{bmatrix}, \quad J_2 = \begin{bmatrix} 0 & I_{(L-1)m} & 0 & 0 \\ 0 & 0 & 0 & I_{(L-1)p} \end{bmatrix}.$$

It is clear that $sJ_1 - J_2$ has full row rank for every $s \in \mathbb{C}$. Together with the full row rank of Γ , it follows that $sE_0 - A_0$ has full row rank for every $s \in \mathbb{C}$. The assertion follows with Proposition 4. \square

Let $w \in \mathcal{B} \cap H^{L-1}(\mathcal{I}, \mathbb{R}^{m+p})$. Then by Lemma 2 there is $\mathbf{g} \in L^2(\mathcal{I}, \mathbb{R}^{L(m+p)})$ such that (4) holds. Given a unimodular embedding G of $sE_0 - A_0$, one has

$$G\left(\frac{d}{dt}\right)\mathbf{g} = \begin{bmatrix} \frac{d}{dt}E_0 - A_0 \\ K \end{bmatrix} \mathbf{g} = \begin{bmatrix} 0 \\ \ell \end{bmatrix},$$

where $\ell := K\mathbf{g}$. By inverting G , one arrives at an image representation (2),

$$w = \begin{bmatrix} \Gamma_{\bar{u}} \\ \Gamma_{\bar{y}} \end{bmatrix} G^{-1}\left(\frac{d}{dt}\right) \begin{bmatrix} 0 \\ \ell \end{bmatrix} = \begin{bmatrix} \Gamma_{\bar{u}} \\ \Gamma_{\bar{y}} \end{bmatrix} G^{-1}\left(\frac{d}{dt}\right) \begin{bmatrix} 0 \\ I \end{bmatrix} \ell. \quad (9)$$

3.2. Staircase form. To construct a unimodular embedding, we transform the pencil $sE_0 - A_0$ corresponding to (6) into *staircase form* using the algorithm described in [13]. The staircase form reveals the Kronecker canonical structure of the pencil. Under the conditions of Corollary 5, there are orthogonal matrices Q, Z such that

$$Q^\top(sE_0 - A_0)Z = sE_1 - A_1 = \begin{bmatrix} -A_{1,1} & sE_{1,2} - A_{1,2} & \cdots & sE_{1,k} - A_{1,k} \\ \ddots & \ddots & & \vdots \\ & -A_{k-1,k-1} & sE_{k-1,k} - A_{k-1,k} & \\ & & & -A_{k,k} \end{bmatrix},$$

where $A_{i,i}$, $i = 1, \dots, k+1$, are upper-triangular with full row rank, while $E_{i,i+1}$, $i = 1, \dots, k$, have full column rank, see [13, Prop. 1] and [1]. A numerically stable algorithm to calculate the staircase form is described in [13].

The pencil $(sE_1 - A_1)$ can be easily embedded in a unimodular pencil. Corresponding to each $A_{i,i}$, find a matrix C_i such that

$$\tilde{A}_{i,i} := \begin{bmatrix} A_{i,i} \\ K_i \end{bmatrix}$$

is upper-triangular and invertible, i.e., let K_i be the lower part of a truncated identity matrix. Consider the embedding of $(sE_1 - A_1)$ into the pencil $(sE_2 - A_2) =$

$[sE_1^\top - A_1^\top \quad \tilde{K}^\top]^\top$, with $\tilde{K} = -\text{diag}(K_1, \dots, K_k)$. Let P be the permutation matrix such that $(sE_3 - A_3) = P(E_2 - sA_2)$, which is of the form

$$sE_3 - A_3 = \begin{bmatrix} -\tilde{A}_{1,1} & \begin{bmatrix} sE_{1,2} - A_{1,2} \\ 0 \end{bmatrix} & & \begin{bmatrix} sE_{1,k} - A_{1,k} \\ 0 \end{bmatrix} \\ & \ddots & \ddots & \vdots \\ & & -\tilde{A}_{k-1,k-1} & \begin{bmatrix} sE_{k-1,k} - A_{k-1,k} \\ 0 \end{bmatrix} \\ & & & -\tilde{A}_{k,k} \end{bmatrix}.$$

Note that A_3 is upper-triangular and invertible. The matrix E_3 is nilpotent and the same holds, therefore, for $N := E_3 A_3^{-1}$. Let $\eta \in \mathbb{N}$ be the nilpotency index of N , i.e., $N^{\eta-1} \neq 0$ and $N^\eta = 0$. Then the inverse of the pencil $(sE_3 - A_3)$ is given by the polynomial matrix

$$(sE_3 - A_3)^{-1} = A_3^{-1}(sN - I)^{-1} = -A_3^{-1} \sum_{j=0}^{\eta-1} s^j N^j$$

and, hence, $sE_3 - A_3$ is unimodular.

3.3. Image representation. The next theorem combines the previous findings.

Theorem 6. *Under the assumption of Corollary 5, consider the decomposition (5), and let $sE_3 - A_3$ be the pencil obtained from the staircase algorithm together with the unimodular embedding using the orthogonal matrices Z , Q and P from Section 3.2. Then the matrix $M(s)$ given via*

$$M(s) = - \begin{bmatrix} \Gamma_{\bar{u}} \\ \Gamma_{\bar{y}} \end{bmatrix} Z A_3^{-1} \sum_{j=0}^{n-1} s^j (E_3 A_3^{-1})^j P \begin{bmatrix} 0 \\ I \end{bmatrix} \quad (10)$$

defines an image representation of \mathcal{B} of the form (2).

Proof. A straightforward calculation shows that

$$G(s) := \begin{bmatrix} sE_0 - A_0 \\ \tilde{K} Z^\top \end{bmatrix} = \begin{bmatrix} Q \\ I \end{bmatrix} P^\top (sE_3 - A_3) Z^\top \quad (11)$$

is a unimodular embedding of the pencil $sE_0 - A_0$ corresponding to (6) with inverse

$$G(s)^{-1} = -Z \left(A_3^{-1} \sum_{j=0}^{n-1} s^j (E_3 A_3^{-1})^j \right) P \begin{bmatrix} Q^\top & I \end{bmatrix}.$$

The assertion follows together with (9). \square

Involving only orthogonal transformations, the calculation of the staircase form is numerically stable, especially in the presence of noisy or perturbed data. The inversion of A_3 during the computation of the image representation, however, is highly sensitive to data corruption; a strategy is discussed in Section 4.

3.4. Gramians from noisy data. A major challenge for the application of the method discussed arises from the fact that the data matrix Γ contains higher-order derivatives of the input and output signals contained in $\text{col}(\bar{u}, \bar{y})$, which are typically corrupted by noise. However, the algebraic differentiators in [11] offer an efficient and robust solution to this problem. A concise overview of algebraic differentiators is provided in the appendix.

In the following we show the invariance of persistency of excitation under convolution with a suitable filter kernel.

Assumption 1. Let $g : \mathbb{R} \rightarrow \mathbb{R}$ be a bounded, $(L-1)$ -times continuously differentiable function satisfying the commutation property $\frac{d^k}{dt^k}(f*g) = (f^{(k)}*g) = (f*g^{(k)})$ for every $f \in H^{L-1}(\mathcal{I}, \mathbb{R})$ and all $k = 1, \dots, L-1$, and whose Fourier transform $\mathcal{F}g$ has only isolated zeros.

Lemma 7. Consider $L \in \mathbb{N}$, $L \geq 1$, and let g satisfy Assumption 1. A signal $\bar{u} \in H^{L-1}(\mathcal{I}, \mathbb{R}^m)$ is persistently exciting of order L if and only if $\tilde{u} := \bar{u} * g$ is persistently exciting of order L . In this case, given \bar{y} such that $\text{col}(\bar{u}, \bar{y}) \in \mathcal{B}$ with $\tilde{y} := \bar{y} * g$, the Gramians Γ in Lemma 2 and $\tilde{\Gamma} := \int_{\mathcal{I}} \tilde{W}(s) \tilde{W}^{\top}(s) ds$ with $\tilde{W} = \text{col}(\tilde{u}, \dots, \tilde{u}^{(L-1)}, \tilde{y}, \dots, \tilde{y}^{(L-1)})$ share the same image and kernel.

The proof of the lemma is given in Appendix B.

The kernels of algebraic differentiators as defined in Appendix A satisfy Assumption 1. The Fourier-domain condition stated in Assumption 1 can be checked using frequency-domain analysis, which also provides insights into the associated noise-attenuation characteristics [7], [12], [14]. The condition that $\mathcal{F}g$ has only isolated zeros ensures that the kernel does not annihilate entire frequency bands. Consequently, the convolution with g preserves almost all frequency components of the signal.

Hence, derivatives of u and y estimated using algebraic differentiators can be used to construct $\tilde{\Gamma}$ as defined in Lemma 7. The invariance of image and kernel implies that, in all preceding computations where the Gramian Γ appears, it can be replaced by $\tilde{\Gamma}$ without affecting the results, cf. Remark 3. In particular, the matrix M in (10) can be constructed solely from noisy data for a data-based prediction.

4. NUMERICAL EXPERIMENTS

We first describe how to generate persistently exciting inputs using random splines. Then, we use singular value decomposition (SVD) to compute the matrix M in (10). Finally, we present simulation results.

Generation of random persistently exciting inputs. Let m be the number of components of the input u of system (1), L the spline degree, N the number of interpolation knots, $[t_{\min}, t_{\max}]$, $t_{\min} < t_{\max}$, a time interval, and $A > 0$ an amplitude parameter. Define a uniform grid $t_j = t_{\min} + \frac{j}{N-1}(t_{\max} - t_{\min})$ for $j = 0, \dots, N-1$, and draw a random matrix $Y \in \mathbb{R}^{m \times N}$ with i.i.d. entries $Y_{i,j} \sim \text{Unif}([-A, A])$. For each $i = 1, \dots, m$, construct the spline S_i of degree L satisfying $S_i(t_j) = Y_{i,j}$. The input signal is defined as $\bar{u}(t) = \text{col}(S_1(t), \dots, S_m(t))$, where A determines its amplitude.

The next lemma, proved in Appendix C, justifies this construction.

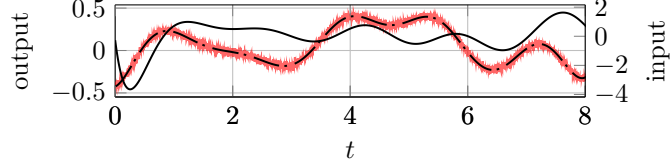


FIGURE 1. Evolution of input \bar{u} (—), output \bar{y} (— · —) and disturbed output \bar{y}_η (—) with SNR = 20.37 dB.

Lemma 8. Suppose $m = 1$ and $L < N$. Consider uniform grid points t_0, \dots, t_{N-1} together with i.i.d. samples $Y_0, \dots, Y_{N-1} \sim \text{Unif}([-A, A])$, $A > 0$. Let S be the spline of degree L satisfying $S(t_i) = Y_i$, $i = 0, \dots, N-1$. Then, with probability one, S is persistently exciting of order L .

Regularized pseudo-inverse via SVD. Generating the polynomial matrix M in (10) requires the inverse of a possible ill-conditioned matrix A_3 . Using the singular value decomposition $A_3 = U\Sigma V^\top$, where $\Sigma = \text{diag}(s_1, s_2, \dots)$ contains the singular values, classical Tikhonov regularization is applied for constructing a regularized pseudo-inverse $A_{\text{reg}}^\dagger = V \text{diag}(s_1^{\text{reg}}, s_2^{\text{reg}}, \dots) U^\top$, where $s_i^{\text{reg}} = s_i/(s_i^2 + \lambda_{\text{reg}})$, with λ_{reg} the regularization parameter (see, e.g., [6]). The inverse of A_3 in (10) is then replaced by A_{reg}^\dagger .

Simulation results and discussion. Consider the system

$$\begin{aligned} \dot{x}(t) &= \begin{bmatrix} 0 & 1 & 0 \\ -1 & 0 & 1 \\ 0 & 0 & -2 \end{bmatrix} x(t) + \begin{bmatrix} 0 \\ 0 \\ 1 \end{bmatrix} u(t), \\ y(t) &= [1 \ 0 \ 1] x(t), \end{aligned}$$

with state $x(t) \in \mathbb{R}^3$, input $u(t) \in \mathbb{R}$, and output $y(t) \in \mathbb{R}$.

The persistently exciting input–output trajectory on the interval $[t_{\min}, t_{\max}]$ is sampled uniformly with step size t_s , resulting in N samples. A disturbed measurement $\bar{y}_\eta(t_i) = \bar{y}(t_i) + \eta_i$, where η_i , $i \in \mathbb{N}$, is a zero-mean white Gaussian i.i.d. sequence, is used for data-based prediction, and \bar{y} is the output corresponding to the persistently exciting input \bar{u} . The variance of the noise sequence η_i is chosen such that the signal-to-noise ratio (SNR) defined as

$$\text{SNR} = 10 \log_{10} \left(\sum_{i=1}^N |y(t_i)|^2 / \sum_{i=1}^N |\eta_i|^2 \right) \quad (12)$$

corresponds to a desired value, where N is the number of samples in $[t_{\min}, t_{\max}]$. The signals \bar{u} and \bar{y}_η are then filtered using an algebraic differentiator to approximate the required derivatives. The differentiators are designed and discretized using the toolbox [15], where the trapezoidal rule is employed for numerical integration. The simulations use the parameter values $t_s = 10^{-3}$, $\alpha_{\text{diff}} = \beta_{\text{diff}} = 8$, $N_{\text{diff}} = 0$, $T_{\text{diff}} = 84 t_s$, $\lambda_{\text{reg}} = 10^{-8}$, $t_{\min} = 0$, $t_{\max} = 3\pi$, $N = 14$, and $L = 7$, where the subscript diff denotes parameters of the differentiator as introduced in Appendix A.

An input–output trajectory is predicted using the data-driven image representation with a chosen ℓ , defined as a linear combination of trigonometric functions. For benchmarking, an estimate \hat{x} of the state is reconstructed from the predicted

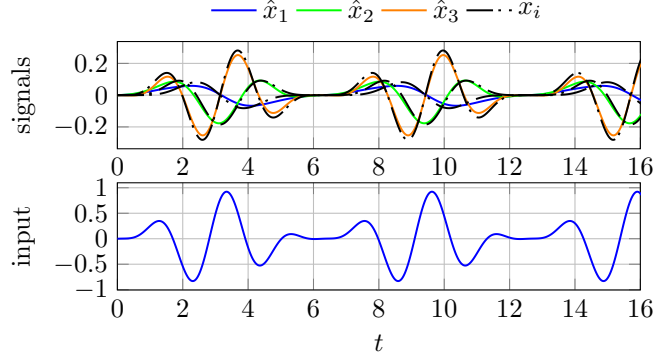


FIGURE 2. Time evolution of the data-based state prediction using the data from Fig. 1 with respect to the true state and the corresponding input trajectory.

input–output trajectory using the Kalman observability matrix, while a reference state trajectory x is obtained by simulating system (1) with a high-accuracy solver. The initial condition for both trajectories is set to $x(0) = \hat{x}(0) = [0 \ 0 \ 0]^\top$. Let $X = [x(t_1) \ \dots \ x(t_N)]$ and $\hat{X} = [\hat{x}(t_1) \ \dots \ \hat{x}(t_N)]$. For quantitative accuracy assessment, define the relative error in the Frobenius norm

$$E(x, \hat{x}) = \|S^{-1}(\hat{X} - X)\|_F \|S^{-1}X\|_F^{-1}, \quad (13)$$

where the matrix $S = \text{diag}(s_1, s_2, \dots, s_n)$ scales each state x_i using its sample standard deviation.

Fig. 1 shows the evolution of the persistently exciting input and output trajectories for an example experiment, referred to as Experiment I. The evolution of the predicted state trajectory \hat{x} using the data-based image representation (10) is shown in Fig. 2 and demonstrates accurate prediction performance. The relative error (13) is $E(x, \hat{x}) = 0.26$. For this experiment the SNR = 20.37 dB, indicating a significant noise level.

Fig. 3 shows the evolution of the persistently exciting input and output trajectories for another experiment, referred to as Experiment II, with a higher SNR = 80.44 dB, yet the predicted state trajectory \hat{x} in Fig. 4 exhibits larger deviations from the true state with a relative error (13) of $E(x, \hat{x}) = 0.41$.

To further analyze performance, we conducted 1500 experiments with randomly drawn interpolation knots and prescribed noise levels. Fig. 5 shows the relative error (13) versus SNR. While prediction error generally decreases with SNR, indicating robustness, some high-SNR experiments yield larger errors than low-SNR cases, showing that input trajectory quality can be more influential than SNR alone.

5. CONCLUSION AND OUTLOOK

In this note, we have derived a numerically stable, data-driven method to obtain an image representation of an unknown continuous-time LTI system, based on a continuous-time version of Willems et al.’s fundamental lemma. We have employed algebraic differentiators to estimate required derivatives and have proven that the essential excitation conditions are preserved under this derivative approximation

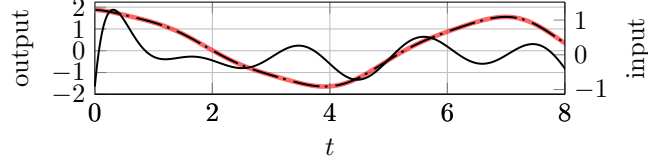


FIGURE 3. Evolution of input \bar{u} (—), output \bar{y} (---) and disturbed output \bar{y}_η (—) with SNR = 80.44 dB.

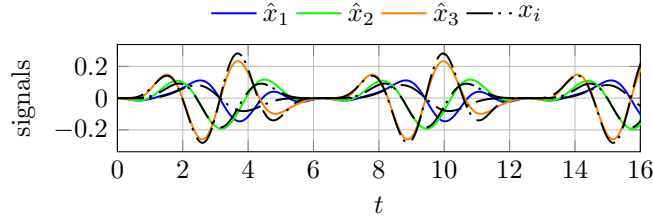


FIGURE 4. Time evolution of the data-based state prediction using the data from Fig. 3 with respect to the true state for the input trajectory from Fig. 2.

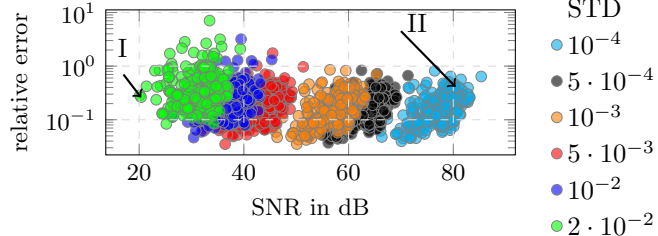


FIGURE 5. Relative error (13) versus SNR (12) for 1500 experiments using randomly sampled interpolation knots for the input generation and different random noise sequences, colored by noise STD. Letters I and II correspond to results in Figs. 2 and 4.

scheme. Simulations confirm the effectiveness of the proposed approach, even under significant measurement noise. Future work should address an extension to systems with multiple outputs and the design of input trajectories that ensure a desired prediction accuracy. Additionally, the obtained results may serve for direct continuous-time data-driven control methods.

APPENDIX A. ALGEBRAIC DIFFERENTIATORS

Consider an interval $\mathcal{I}_t = [t - T_{\text{diff}}, t] \subset \mathbb{R}$, with $T_{\text{diff}} > 0$. By mapping this interval to $[-1, 1]$, a square-integrable function f defined on \mathcal{I}_t can be approximated using Jacobi polynomials $P_{N_{\text{diff}}}^{(\alpha_{\text{diff}}, \beta_{\text{diff}})}$ of degree N_{diff} , which form an orthogonal basis

with respect to the weight

$$w(\tau) = \begin{cases} (1-\tau)^{\alpha_{\text{diff}}}(1+\tau)^{\beta_{\text{diff}}}, & \tau \in (-1, 1) \\ 0, & \text{otherwise.} \end{cases}$$

The inner product associated with this weight is defined by

$$\langle p, q \rangle_w = \int_{-1}^1 p(\tau) q(\tau) w(\tau) d\tau,$$

and the corresponding norm is defined by $\|p\|_w^2 = \langle p, p \rangle_w = \int_{-1}^1 p(\tau)^2 w(\tau) d\tau$.

For $\min\{\alpha_{\text{diff}}, \beta_{\text{diff}}\} > n - 1$, $n \geq 0$, a generalized Fourier expansion of order N_{diff} yields the estimate

$$\hat{f}^{(n)}(t) = \int_{t-T_{\text{diff}}}^t g^{(n)}(t-\tau) f(\tau) d\tau = (g^{(n)} * f)(t) \quad (14)$$

for $f^{(n)}(t)$, with $g(\tau) = \frac{2}{T_{\text{diff}}} w(\nu(\tau)) \sum_{j=0}^{N_{\text{diff}}} \frac{p_j(\vartheta_{\text{diff}})}{\|p_j\|_w^2} p_j(\nu(\tau))$, $\nu(\tau) = 1 - 2\tau/T_{\text{diff}}$, window length T_{diff} , Jacobi polynomial $p_j = P_j^{(\alpha_{\text{diff}}, \beta_{\text{diff}})}$ with parameters α_{diff} and β_{diff} , expansion order N_{diff} , and the scalar ϑ_{diff} parameterizing the approximation delay (see, e.g., [14] for more details). Notice that $g^{(n)} * f = g * f^{(n)}$.

APPENDIX B. CONVOLUTED GRAMIANS

Before we prove Lemma 7 in this section, we state and prove the next auxiliary result.

Lemma 9. *Let g satisfy Assumption 1. Consider $w \in H^{L-1}(\mathcal{I}, \mathbb{R}^d)$. Then for $W := \text{col}(w, \dots, w^{(L-1)})$ and $W_g := \text{col}(w * g, \dots, (w * g)^{(L-1)})$ the Gramians*

$$\Gamma := \int_{\mathcal{I}} W(s) W(s)^\top ds, \quad \Gamma_g := \int_{\mathcal{I}} W_g(s) W_g(s)^\top ds$$

have the same image and kernel. In particular, $\eta \in \ker \Gamma = \ker \Gamma_g$ if and only if $W^\top \eta = W_g^\top \eta = 0$ a.e.

Proof. Observe that $W_g = W * g = g * W$. We show $\ker \Gamma = \ker \Gamma_g$. Note that $\Gamma \eta = 0$ if and only if $\eta^\top \Gamma \eta = 0$, which is equivalent to $W^\top \eta = 0$ a.e.; similarly for Γ_g and W_g . Let $\eta \in \ker \Gamma$ and, therefore, $W_g^\top \eta = g * (W^\top \eta) = 0$ a.e. This implies $\eta \in \ker \Gamma_g$. Let $\eta \in \ker \Gamma_g$ and, therefore, $W_g^\top \eta = 0$ a.e. Applying the Fourier transform one sees

$$0 = \mathcal{F}(W_g^\top \eta) = \mathcal{F}(g * W^\top \eta) = \mathcal{F}g \cdot \mathcal{F}(W^\top \eta) \quad \text{a.e.}$$

Since $\mathcal{F}g$ has only isolated zeros this implies $\mathcal{F}(W^\top \eta) = 0$ a.e. and, hence, $W^\top \eta = 0$ a.e. This yields $\eta \in \ker \Gamma$.

Since both Gramians are symmetric matrices, we find

$$\text{im } \Gamma = (\ker \Gamma)^\perp = (\ker \Gamma_g)^\perp = \text{im } \Gamma_g. \quad \square$$

Now we turn to Lemma 7. We apply Lemma 9 with $w = \bar{u}$. By definition, \bar{u} is persistently exciting of order L if and only if $W^\top \eta = 0$ implies $\eta = 0$, which by Lemma 9 is equivalent to $\ker \Gamma = \{0\}$; a similar statement is true for $\tilde{u} = \bar{u} * g = w_g$ and Γ_g . This shows the first assertion in Lemma 7. The second claim in Lemma 7 follows immediately by applying Lemma 9 with $w = \text{col}(\bar{u}, \bar{y})$.

APPENDIX C. PERSISTENTLY EXCITING SPLINES

In this section we prove Lemma 8, by showing that the complementary event Ω_0 , that the spline S is not persistently exciting of order L , has probability zero. Assume that S is not persistently exciting of order L . It is not difficult to see that this implies that the restriction of S to any subinterval is not persistently exciting of order L either.

On each interval $\mathcal{I}_i := (t_i, t_{i+1})$, the spline S coincides with a polynomial $p_i \in \mathbb{R}[s]$ of degree at most L . Since polynomials of degree L are persistently exciting of order L (see [17, Ex. 18]), in fact, $\deg p_i \leq L - 1$ for $i = 0, \dots, N - 1$. Note that the spline S is $(L - 1)$ -times continuously differentiable. In particular, $p_i^{(j)}(t_i) = S^{(j)}(t_i) = p_{i+1}^{(j)}(t_i)$ for $i = 0, \dots, N - 2$ and $j = 0, \dots, L - 1$. Because a degree- $(L - 1)$ polynomial is uniquely determined by its first L derivatives at a single point, all polynomials p_i coincide. Therefore, S is a polynomial on $[t_0, t_{N-1}]$ with $\deg S \leq L - 1$. This implies $\Omega_0 \subset \Omega \cap [-A, A]^N$, where

$$\Omega = \left\{ \begin{bmatrix} Y_0 & \dots & Y_{N-1} \end{bmatrix}^\top \in \mathbb{R}^N \middle| \begin{array}{l} \exists p \in \mathbb{R}[s], \deg p \leq L - 1, \\ p(t_i) = Y_i, \quad i = 0, \dots, N - 1 \end{array} \right\}.$$

We show that Ω has Lebesgue measure zero. Note that the space of real polynomials of degree at most $L - 1$ is isometric to \mathbb{R}^L . Let Π denote the corresponding isomorphism and δ be the point-evaluation operator $\delta : \mathbb{R}[s] \rightarrow \mathbb{R}^N$, $p \mapsto [p(t_0) \ \dots \ p(t_{N-1})]^\top$. The dimension of $\Omega = \delta(\Pi(\mathbb{R}^L))$ is bounded above by L , which by $L < N$ makes Ω a proper linear subspace of \mathbb{R}^N and, thus, it is a zero-set with respect to the N -dimensional Lebesgue measure λ . Consequently, the probability of the event Ω_0 is bounded by

$$\mathbf{P}(\Omega_0) \leq \int_{\Omega \cap [-A, A]^N} \frac{1}{2A} d\lambda = 0. \quad \square$$

REFERENCES

- [1] T. BEELEN AND P. VAN DOOREN, *A pencil approach for embedding a polynomial matrix into a unimodular matrix*, SIAM Journal on Matrix Analysis and Applications, 9 (1988), pp. 77–89.
- [2] J. COULSON, J. LYGEROS, AND F. DÖRFLER, *Data-enabled predictive control: In the shallows of the DeePC*, in 18th European Control Conference (ECC), 2019, pp. 307–312.
- [3] C. DE PERSIS AND P. TESI, *Formulas for data-driven control: Stabilization, optimality, and robustness*, IEEE Transactions on Automatic Control, 65 (2020), pp. 909–924.
- [4] F. DÖRFLER, J. COULSON, AND I. MARKOVSKY, *Bridging direct and indirect data-driven control formulations via regularizations and relaxations*, IEEE Transactions on Automatic Control, 68 (2022), pp. 883–897.
- [5] T. FAULWASSER, R. OU, G. PAN, P. SCHMITZ, AND K. WORTHMANN, *Behavioral theory for stochastic systems? A data-driven journey from Willems to Wiener and back again*, Annual Reviews in Control, (2023), pp. 92–117.
- [6] G. H. GOLUB AND C. F. VAN LOAN, *Matrix Computations*, Johns Hopkins University Press, Baltimore, 2013.
- [7] L. KILTZ AND J. RUDOLPH, *Parametrization of algebraic numerical differentiators to achieve desired filter characteristics*, in 52nd IEEE Conference on Decision and Control (CDC), 2013, pp. 7010–7015.
- [8] V. G. LOPEZ AND M. A. MÜLLER, *On a continuous-time version of Willems' lemma*, in 61st IEEE Conference on Decision and Control (CDC), 2022, pp. 2759–2764.
- [9] V. G. LOPEZ, M. A. MÜLLER, AND P. RAPISARDA, *An input-output continuous-time version of Willems' lemma*, IEEE Control Systems Letters, 8 (2024), pp. 916–921.

- [10] I. MARKOVSKY AND F. DÖRFLER, *Behavioral systems theory in data-driven analysis, signal processing, and control*, Annual Reviews in Control, 52 (2021), pp. 42–64.
- [11] M. MBOUP, C. JOIN, AND M. FLEISS, *Numerical differentiation with annihilators in noisy environment*, Numerical Algorithms, 50 (2009), pp. 439–467.
- [12] M. MBOUP AND S. RIACHY, *A frequency domain interpretation of the algebraic differentiators*, IFAC Proceedings Volumes, 47 (2014), pp. 9147–9151.
- [13] C. OARĀ AND P. VAN DOOREN, *An improved algorithm for the computation of structural invariants of a system pencil and related geometric aspects*, Systems & Control Letters, 30 (1997), pp. 39–48.
- [14] A. OTHMANE, L. KILTZ, AND J. RUDOLPH, *Survey on algebraic numerical differentiation: Historical developments, parametrization, examples, and applications*, International Journal of Systems Science, 53 (2022), pp. 1848–1887.
- [15] A. OTHMANE AND J. RUDOLPH, *Algdiff: an open source toolbox for the design, analysis and discretisation of algebraic differentiators*, at-Automatisierungstechnik, 71 (2023), pp. 612–623.
- [16] P. RAPISARDA, M. ÇAMLIBEL, AND H. VAN WAARDE, *A “fundamental lemma” for continuous-time systems, with applications to data-driven simulation*, Systems & Control Letters, 179 (2023), p. 105603.
- [17] P. SCHMITZ, T. FAULWASSER, P. RAPISARDA, AND K. WORTHMANN, *A continuous-time fundamental lemma and its application in data-driven optimal control*, Systems & Control Letters, 194 (2024), p. 105950.
- [18] J. C. WILLEMS AND J. W. POLDERMAN, *Introduction to mathematical systems theory: A behavioral approach*, vol. 26, Springer Science & Business Media, 1997.
- [19] J. C. WILLEMS, P. RAPISARDA, I. MARKOVSKY, AND B. L. M. DE MOOR, *A note on persistency of excitation*, Systems & Control Letters, 54 (2005), pp. 325–329.

SYSTEMS MODELING AND SIMULATION, SAARLAND UNIVERSITY, SAARBRÜCKEN, GERMANY

Email address: amine.othmane@uni-saarland.de

OPTIMIZATION-BASED CONTROL GROUP, TECHNISCHE UNIVERSITÄT ILMENAU, ILMENAU, GERMANY

Email address: philipp.schmitz@tu-ilmenau.de

OPTIMIZATION-BASED CONTROL GROUP, TECHNISCHE UNIVERSITÄT ILMENAU, ILMENAU, GERMANY

Email address: karl.worthmann@tu-ilmenau.de

SYSTEMS MODELING AND SIMULATION, SAARLAND UNIVERSITY, SAARBRÜCKEN, GERMANY

Email address: kathrin.flasskamp@uni-saarland.de